Mechanisms of Performance Degradation of (La,Sr)(Co,Fe)$O_{3-\delta}$ Solid Oxide Fuel Cell Cathodes

Hongqian Wang,[a] Kyle J. Yakal-Kremski,[a,c] Ted Yeh,[a,d] Ghislain M. Rupp,[b] Andreas Limbeck,[b] Jürgen Fleig,[b,*] and Scott A. Barnett[a,*,z]

[a]*Department of Materials Science and Engineering, Northwestern University, Evanston, Illinois 60208, USA*
[b]*Institute of Chemical Technologies and Analytics, Vienna University of Technology, Vienna A-1060, Austria*

Symmetric cells with porous $La_{0.6}Sr_{0.4}Co_{0.2}Fe_{0.8}O_{3-\delta}$ (LSCF) electrodes on $Gd_{0.1}Ce_{0.9}O_{1.95}$ (GDC) electrolytes were aged at 800°C for 800 hours in ambient air. Electrochemical impedance spectroscopy (EIS) measurements performed periodically at 700°C showed a continuous increase of the polarization resistance from 0.15 to 0.34 $\Omega \cdot cm^2$. Three-dimensional (3D) tomographic analysis using focused ion beam–scanning electron microscopy (FIB-SEM) showed negligible changes due to the ageing, suggesting that the observed resistance increase was not caused by electrode morphological evolution. However, an increased amount, by a factor of 3, of a water-soluble Sr rich surface phase on the aged LSCF electrode was detected by an etching procedure coupled with inductively coupled plasma-optical emission spectrometry (ICP-OES). The electrochemical analysis in combination with the microstructural parameters determined by FIB-SEM was used to examine the effect of Sr segregation on the rate of oxygen surface exchange, based on the Adler-Lane-Steele (ALS) model.

Manuscript submitted February 10, 2016; revised manuscript received March 16, 2016. Published March 26, 2016. This article is a version of Paper 1530 from the San Diego, California, Meeting of the Society, May 29- June 2, 2016.

Mixed ionic-electronic conducting (MIEC) materials such as $La_{0.6}Sr_{0.4}Co_{0.2}Fe_{0.8}O_{3-\delta}$ (LSCF) have been studied and developed as solid oxide fuel cell (SOFC) cathodes, due to their high activity for the oxygen reduction reaction at intermediate temperatures (<800°C).[1–6] However, a number of MIEC materials including LSCF exhibit Sr surface segregation, which has been proposed to hinder the oxygen surface exchange process.[7–11] This is believed to be an important issue for the stability of advanced SOFCs utilizing MIEC cathodes. Still, most of the Sr segregation observations have been made on thin film samples, where it is straightforward to measure surface composition using techniques such as X-ray photoelectron spectroscopy (XPS), Auger electron spectroscopy (AES), and secondary ion mass spectrometry (SIMS).[12–15] Recently Rupp et al.[16] reported a novel technique utilizing chemical etching with on-line inductively coupled plasma optical emission spectrometry (ICP-OES) detection to successfully quantify Sr-rich surface phases on dense $La_{0.6}Sr_{0.4}CoO_{3-\delta}$ (LSC) thin films. There is only one report of a measurement of a practical porous LSCF electrode that showed Sr segregation, measured via XPS, along with electrochemical performance degradation.[11]

The distinction between thin film and bulk electrode samples is potentially important. Thin films are often characterized by columnar growth with very high grain boundary densities, they may exhibit significant stress, and the thermal history is usually very different from that of porous electrodes (preparation mostly below 800°C). Although the measured properties of well-prepared polycrystalline thin-film electrodes normally agree reasonably well with values from bulk materials,[17] in some cases such as epitaxial thin film electrodes, properties may deviate significantly.[18] Also, SOFC stacks with LSCF cathodes have been shown to provide reasonably stable long-term performance,[19] an observation that appears to be at odds with the Sr segregation and related degradation observed for thin-film LSCF.

In this work, we investigated the degradation mechanisms, especially Sr surface segregation, of porous LSCF cathodes. LSCF symmetric-electrode cells with $Gd_{0.1}Ce_{0.9}O_{1.95}$ (GDC) electrolytes were maintained at an elevated SOFC operating temperature of 800°C for extended times, without current/polarization. Electrochemical degradation was monitored using impedance spectroscopy, while morphological changes of the electrode and Sr surface segregation were examined using a combination of three-dimensional (3D) tomography via focused ion beam-scanning electron microscopy (FIB-SEM) and surface composition measurements using XPS and chemical etching with ICP-OES detection. The chemical dissolution method,[16] when combined with LSCF electrode surface area measured from 3D image data, provided a quantitative measure of Sr surface coverage. The 3D imaging also showed that there were no observed changes by coarsening or sintering of the LSCF electrode microstructure, and this is thus ruled out as an influence which could be affecting electrochemical performance. The Adler-Lane-Steele (ALS) model[20] was applied, again making use of 3D image data, to examine the effect of Sr surface segregation on the oxygen surface exchange and diffusion processes.

Experimental

Cell preparation.—Symmetric-electrode cells were prepared starting with ~0.5-mm-thick $Gd_{0.1}Ce_{0.9}O_{1.95}$ (GDC) electrolytes. The electrolytes were prepared by uniaxial dry-pressing from GDC powder (NexTech, Ohio) pellets, fired at 1450°C for 6 hours to achieve nearly full density. Identical porous $La_{0.6}Sr_{0.4}Co_{0.2}Fe_{0.8}O_{3-\delta}$ (LSCF) electrodes, with ~15 μm thickness, were applied symmetrically on both sides of the GDC electrolytes. The electrodes were prepared by first making an ink by mixing LSCF powder (Praxair, Washington) with a vehicle (Heraeus V-737) in a three-roll mill, screen printing the ink onto the electrolyte, and firing at 1100°C in ambient air for 1 hour. The electrode cation stoichiometry, analyzed by ICP-OES after completely dissolving several electrodes in HCl, was determined to be $La_{0.61\pm0.01}Sr_{0.39\pm0.01}Co_{0.19\pm0.01}Fe_{0.81\pm0.01}$. Cell preparation was completed by screen printing gold current collector grids on the surfaces of both electrodes.

Electrochemical characterization and life testing.—Electrochemical life tests of the symmetrical cells were carried out in a tube furnace with both electrodes exposed to ambient air. Two identically-prepared cells were placed together in the furnace, but measured separately. The cells were aged at 800°C with no applied current or potential. Electrochemical impedance spectroscopy (EIS) measurements were taken periodically (once per day) after reducing the furnace temperature and stabilizing at 700°C. The entire measurement cycle, from 800°C to 700°C and back, typically took ~1 hour. The measurement temperature (700°C) was chosen as

*Electrochemical Society Member.
[c]Present Address: National Academy of Sciences, Washington, DC 20001, USA.
[d]Present Address: Narrative Science, Chicago, Illinois 60601, USA.
[z]E-mail: s-barnett@northwestern.edu

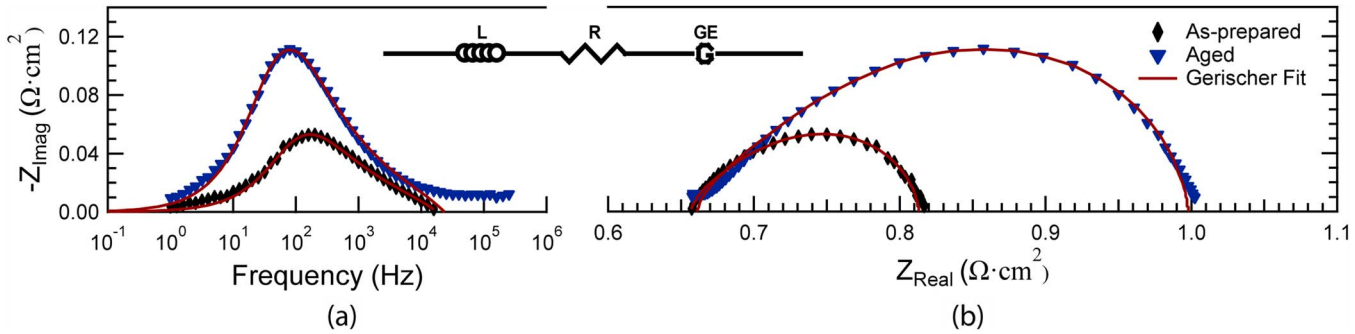

Figure 1. Bode (a) and Nyquist (b) plots of EIS data measured at 700°C in air from an LSCF-electrode symmetrical cell. The "as-prepared" data were taken at the beginning and the "aged" data at the end of the 800-hour life test at 800°C. The data are fitted with an inductor (L), an ohmic resistance (R) and a modified Gerischer element (GE).

a typical LSCF-cathode SOFC operating temperature, whereas the ageing was done at the upper end of the expected operating temperature range, 800°C, in order to accelerate any changes in cell performance. Potentiostatic EIS testing was taken using four lead wires on an IM6 Electrochemical Workstation (ZAHNER, Germany) with a 20 mV AC signal amplitude at a 0 V mean potential, measured over a frequency range of 100 mHz – 100 kHz.

Microstructural characterization.—In order to examine the effect of the thermal ageing on the cell degradation, microstructural analysis was done using 3D FIB-SEM tomography. Identically-prepared cells were compared in the as-prepared state and after ageing. Cells were prepared for FIB-SEM serial sectioning by fracturing, infiltrating with low-viscosity epoxy (Buehler), and polishing, as described in detail elsewhere.[21,22] Analysis was done on a dual-beam Zeiss 1540XB as well as on a FEI Helios. The secondary electron (SE) detector with an accelerating voltage of 2 kV was used; the relatively low energy provided optimal contrast between the epoxy-filled electrode pores and solid phases and prevented sample charging. Image segmentation and 3D reconstruction were done as described elsewhere.[22] Microstructural parameters such as porosity, tortuosity, surface areas and particle size distributions were then calculated based on the 3D data. An as-prepared cell was used as a reference sample, for comparison with the life-tested cells.

Chemical characterization.—The as-prepared and aged cells were fractured into four fragments. The cell fragments were separately stirred for either 10 or 30 minutes in ultrapure H_2O (produced by Barnstead Easypure II (18.2 $M\Omega \cdot cm^{-1}$)). Subsequently, the samples were transferred into a 12 $mol \cdot L^{-1}$ solution of hydrochloric acid until the electrodes were completely dissolved. The ultrapure H_2O and the concentrated HCl solutions were mixed with the appropriate amounts of water/HCl to yield 0.12 $mol \cdot L^{-1}$ solutions for ICP-OES analysis.

A Thermo Scientific iCAP 6500 ICP spectrometer was employed, equipped with a peristaltic pump, nebulizer and cyclone for sample introduction, a quartz torch, an echelle spectrometer, and a charge injection device detector. The RF-power was set to 1200 W. A 0.8 $L \cdot Ar \cdot min^{-1}$ auxiliary and a 12 $L \cdot Ar \cdot min^{-1}$ cooling gas flow were applied. The liquid flow was set to 0.6 $mL \cdot min^{-1}$ and the nebulizer gas flow to 0.7 $L \cdot Ar \cdot min^{-1}$. The following background corrected emission lines were chosen for evaluation: Sr (346.446 nm), La (379.478 nm), Co (228.616 nm; 238.892 nm), Fe (239.562 nm; 259.940 nm). For quantification, certified stock solutions (1000 $mg \cdot L^{-1}$ from Merck KGaA) of La, Sr, Co and Fe were used for the preparation of calibration standards by dilution with 0.12 $mol \cdot L^{-1}$ HCl. Five replicates were measured at an integration time of two seconds for standards and samples.

XPS spectra were collected on a Thermo Scientific ESCALAB 205Xi to determine surface cation changes. Both as-prepared and aged samples were analyzed, with characteristic electron energy windows for all cations, as well as oxygen, collected. Copper tape was used to ground the samples to the stage to prevent sample charging. Gold, present from the current collector, was used as an internal standard for experimental energy offsets, as it is not expected to react with the electrode samples. Comparative analysis was performed by determining the relative integrated intensities for the present peaks for each cation for each sample. Changes in these intensities can suggest differences in relative amounts of valence for particular cations in a sample. However, quantitative analysis between samples, and indeed within a given sample, was not performed due to inconsistent variations between spots, as discussed below. Additionally, cobalt spectra were ignored due to the very low signal to noise ratio, likely due to the low concentration of cobalt in LSCF.

Results

Electrochemical characterization.—Fig. 1 shows the Bode and Nyquist plots of typical EIS data taken before (denoted "as-prepared") and after (denoted "aged") thermal treatment at 800°C for 800 hours. Only one cell is shown here, since the other cell yielded similar results. EIS measurements enabled separation of the LSCF electrode polarization resistance and the GDC electrolyte ohmic resistance. The ohmic resistance (R_{ohm}), attributed primarily to the electrolyte, was measured from the high frequency intercepts with the real axis in the Nyquist plot. The polarization resistance (R_{pol}) was measured as the difference between the intercepts with real axis at low and high frequencies. Fig. 2 shows the R_{pol} and R_{ohm} values obtained from EIS measurements taken periodically during ageing. Data for the two identically-prepared cells are shown. The R_{pol} evolutions are almost identical for the two cells, indicating good cell reproducibility. The difference mainly arises from the R_{ohm}, presumably due to cell-to-cell variations, e.g. slightly different electrolyte thicknesses. The ohmic resistance increases by only 2.6% throughout the test. This may have resulted from slight electrolyte ageing, or minor degradation of the electrical contacts. On the other hand, the polarization resistance increased from 0.15 to 0.34 $\Omega \cdot cm^2$ (∼120%) during the life test.

3D microstructural analysis.—Fig. 3 shows typical FIB-SEM cross-sectional images from the as-prepared (a) and aged (b) cells. Figs. 3c and 3d show the corresponding 3D reconstructions, with LSCF particles in green and the pores transparent. The images show a highly porous structure with considerable local variations – most of the volume consists of a uniform distribution of solid phase with pores, but there are also larger regions devoid of solid phase. Average microstructural parameters obtained from the reconstructions are summarized in Table I. The LSCF tortuosity τ was low, ∼1.2, and did not vary significantly after ageing. The porosity ε was ∼50%, as expected for typical MIEC electrodes, and increased ∼10% after ageing. Since a decrease in porosity is expected after ageing, it seems likely that the increase in ε was an artifact arising from the inhomogeneous porosity distribution, which results in a statistical variation

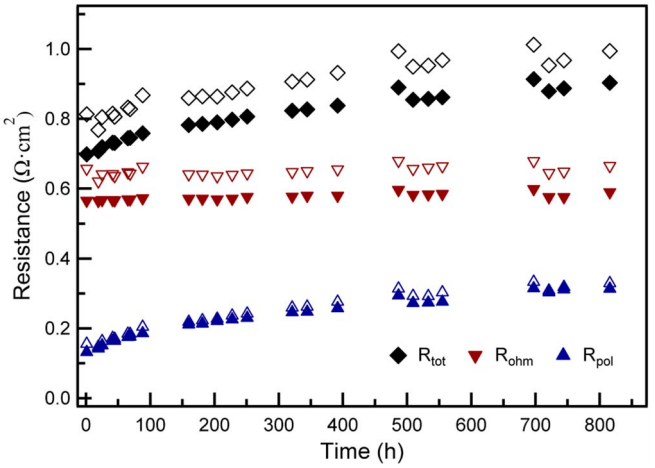

Figure 2. Cell ohmic resistance, polarization resistance, and total resistance versus time, obtained from EIS data from two identically-prepared LSCF symmetric cells at 700°C in air, such as that shown in Fig. 1. The temperature was maintained at 800°C during the life test, except for brief interruptions when the temperature was reduced to 700°C for EIS measurements. The resistances from the two cells are presented in filled and open data points.

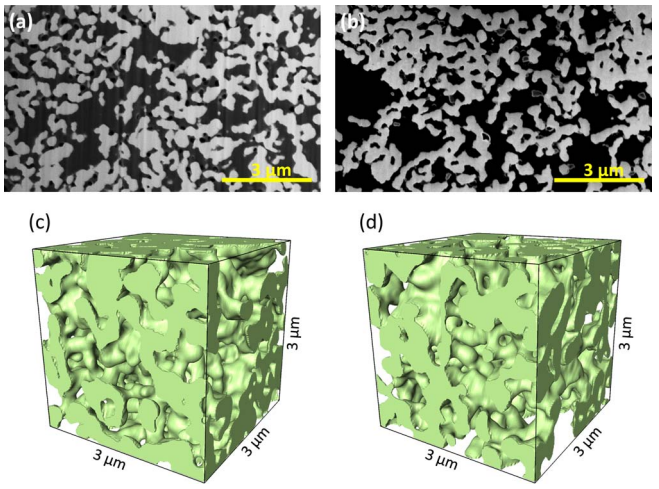

Figure 3. 2D micrographs of the as-prepared (a) and aged (b) LSCF electrodes – black regions are the pore space while the lighter areas are LSCF. The corresponding 3D reconstructions are shown in (c) and (d), with LSCF particles in green and pores transparent. Note that the 3D views in (c) and (d) show smaller regions cropped from the full reconstruction volume, for clarity. The actual reconstruction volumes are 11.55 × 5.25 × 12.3 μm^3 and 9.12 × 7.56 × 9.92 μm^3 for the as-prepared and aged electrodes, respectively.

in the porosity measured at different electrode regions. The LSCF surface area per unit electrode volume, a_v, decreased by ∼10% after ageing. However, this can be attributed almost entirely to the reduced solid volume in that measured volume, as indicated by the higher ε value. The LSCF specific surface area, *a,* provides a more statistically relevant measure of LSCF structure since local porosity variations are cancelled out in dividing a_v by the solid volume. There is only a slight

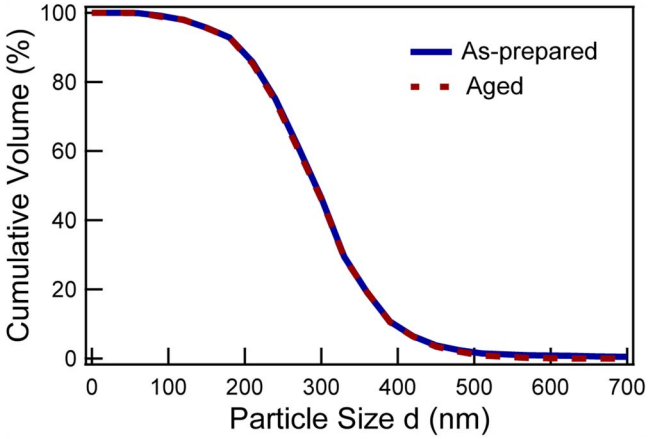

Figure 4. Cumulative particle size distribution of LSCF calculated from 3D tomographic images.

decrease in *a*, from 10.34 μm^{-1} for the as-prepared electrode to 10.30 μm^{-1} for the aged electrode. This 0.4% change is well within the error limit of comparative FIB-SEM tomography measurements.[21] Based on these results, it can be concluded that ageing-induced changes in electrode porosity and surface area are small, ≤10%, and probably much less than that.

Fig. 4 shows the LSCF feature size distributions, obtained from the 3D data using the method reported by Holzer.[23] The size distributions are essentially identical for the as-prepared and aged cells. These results, combined with the negligible change in LSCF specific surface area, makes it reasonable to conclude that there was no significant change in the electrode microstructure due to the thermal ageing. Hence, the measured degradation of the LSCF electrodes under these conditions cannot be explained by coarsening.

Sr surface segregation.—*ICP-OES analysis.*—Fig. 5 summarizes the water-soluble amounts of cations extracted after stirring the as-prepared and aged electrodes for 10 or 30 minutes in ultrapure H_2O. The amount was normalized to the 3D-tomography-derived LSCF surface areas given in Table I. For all samples, large amounts of water-soluble Sr (>1.1 nmol/cm^2) are found in comparison to insignificant amounts of La, Co, Fe cations (<0.05 nmol/cm^2) in the leaching solutions. This is in agreement with the very low water solubility of bulk LSCF but indicates the presence of a water-soluble Sr-rich layer on the surface of as-prepared LSCF electrodes. The amount of Sr found after stirring the as-prepared sample for 10 min is within the measurement error of the samples stirred for 30 min (error bars in Fig. 5 calculated by standard deviation of n = 3 samples). In agreement with Ref. 25, we discuss this additional Sr in terms of SrO layers with a SrO monolayer being defined by a dense homogenous SrO coverage with a (100) orientation (lattice parameter of 0.516 nm). With this assignment, the present measurements indicate 1.04 ± 0.22 monolayers of surface SrO for the as-prepared samples ($7.8 \cdot 10^{14} \pm 1.65 \cdot 10^{14}$ SrO units/cm^2). This suggests that the as-prepared LSCF particles are terminated by a single SrO rocksalt layer. A similar result was obtained by the same method on as-prepared LSC thin films[16,24] and by low energy ion scattering measurements on as-prepared LSCF thin films,[25] despite different thermal history.

Table I. Summary of calculated microstructural parameters for the as-prepared and aged LSCF electrodes.

Microstructural Parameter	As-prepared	800°C Aged	Percent Change
Porosity ε (%)	51.9	56.9	+ 9.6%
LSCF Surface Area per Electrode Volume a_v (μm^{-1})	4.97	4.44	−10.7%
LSCF Specific Surface Area *a* (μm^{-1})	10.34	10.30	−0.4%
LSCF Tortuosity τ	1.18	1.22	+ 3.4%

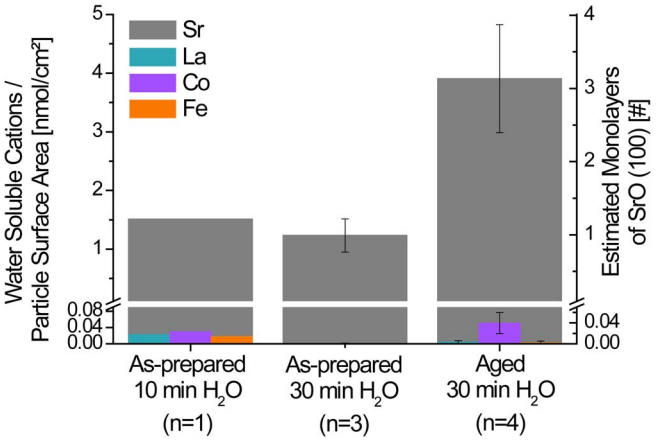

Figure 5. The amounts of Sr, La, Co, and Fe cations dissolved in ultrapure water for the as-prepared and aged cells. The detected amount was normalized by LSCF surface area and the error bars are calculated from standard deviation of the n measurements. From the amount of water soluble Sr nominal numbers of SrO monolayers were estimated.

The aged LSCF electrode surfaces showed a strongly enhanced amount of Sr (from 1.30 ± 0.27 to 3.90 ± 0.92 nmol/cm^2), see Fig. 5. Accordingly, drastic changes of the surface and near-surface composition of the LSCF particles took place upon ageing. Nominally, 3.13 ± 0.22 SrO monolayers on top of the LSCF electrode can be estimated from these results. However, there is also the possibility of an inhomogeneous Sr surface segregation with formation of much thicker islands, cf. results on degraded thin films.[15] Moreover, formation of other secondary phases such as $Sr(OH)_2$ and $SrCO_3$ as reaction products formed with absorbed gas either during ageing or during/after cooling of the samples cannot be excluded, given the favorable free energy of formation of $SrCO_3$ and $Sr(OH)_2$ from SrO. In any case this substantial amount of additional Sr on the surface is expected to modify the oxygen surface exchange kinetics and thus to degrade the electrode performance, see EIS measurements and discussion in the next section.

XPS measurements.—Fig. 6 shows representative XPS spectra, in the regions where the Sr 3d peaks are observed, obtained from the as-prepared and aged LSCF electrodes. The basic peak positions and intensities are similar to those reported previously for LSCF electrodes.[26] There was minor increase at the low energy satellite peak at 131.8 eV after ageing, but it is difficult to attribute this to a change

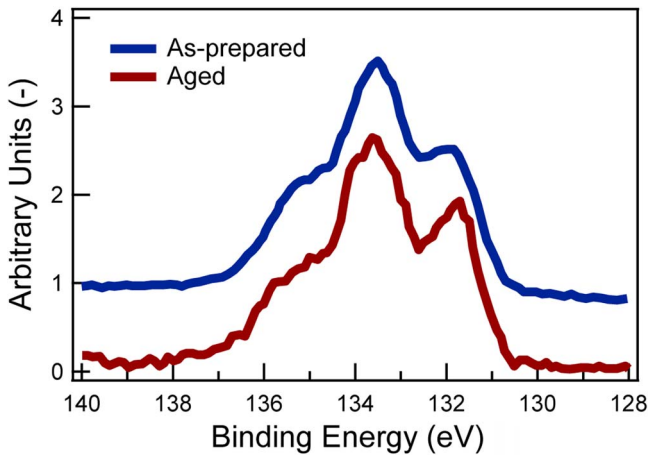

Figure 6. Sr 3d peaks from XPS analysis for the as-prepared and aged LSCF electrodes.

Table II. Summary of kinetic parameters at 700°C determined by ALS model for as-prepared and aged cells.

	As-prepared	800°C Aged	Percent Change	Literature[37]
R_G ($\Omega \cdot cm^2$)	0.15	0.34	-	-
t_G (s)	0.0017	0.0035	-	-
k (cm/s)	5.17E-5	2.26E-5	-56%	1.49E-6
D^* (cm^2/s)	5.27E-10	2.87E-10	-45%	3.04E-9

in Sr surface coverage or Sr cation coordination. Measurements of the other cation peaks, not shown here, also showed peak positions and intensities similar to previous reports.[26] However, the peak intensities were inconsistent between probed X-ray spots, even on the same sample, making it impossible to observe changes in surface composition. It seems reasonable to conclude that the roughness and inhomogeneous porous electrode surface was not ideal for XPS measurements, so only the ICP-OES measurements are discussed below.

Discussion

Based on the above results, it appears that the main change in the LSCF electrodes upon ageing is an increased Sr surface coverage. The results in Electrochemical characterization section show that there is a substantial change in the EIS response due to ageing. Here we analyze the EIS data in an attempt to determine how Sr segregation affects the oxygen reduction reaction. Recently, it has been shown that the oxygen surface exchange rate k and solid-state oxygen diffusion coefficient D^* can be estimated for porous MIEC electrodes by using the ALS model[20] combined with electrode microstructural data.[27,28] As shown in Fig. 1, electrode EIS data could be modeled reasonably well by an equivalent circuit consisting of an inductor (L), an ohmic resistance (R) and a modified Gerischer element (GE). Eq. 1 describes the impedance of the modified Gerischer element,[29] where $\alpha < 1$, which has the similar form as the phenomenological Havriliak-Negami dielectric dispersion relation.[30] This 'fractal' modification of the Gerischer expression gives a much improved model of the low frequency end of the data.

$$Z = R_G \sqrt{\frac{1}{1 + (j\omega t_G)^{\alpha}}} \qquad [1]$$

where R_G is the Gerischer resistance and t_G is the time constant. Fig. 1 shows the fits obtained, which yield the R_G and t_G values, given by the ALS model as:

$$R_G = \frac{RT}{2F^2} \sqrt{\frac{\tau}{(1-\varepsilon)\, a D^* k c_{mc}^2}} \qquad [2]$$

$$t_G = \frac{\chi_v (1-\varepsilon)}{A_0 a k} \qquad [3]$$

where τ is the tortuosity, ε is the porosity, and a is the pore-electrode interfacial area per volume, given in Table I from the FIB-SEM data. The oxygen concentration, c_{mc}, was approximated as 0.083 mol/cm^3 at 700°C as measured by Mizusaki[31] for this LSCF composition. Based on oxygen nonstoichiometry, the oxygen vacancy fraction, χ_v, and the thermodynamic factor, A_0, were estimated to be 0.035 and 1.85, respectively.[27,32,33] With the above quantities known, and R_G and t_G determined from the EIS fitting shown in Fig. 1, k and D^* are calculated from Eqs. 2 and 3. The results are shown in Table II.

The calculated k and D^* values are within the range of reported values for LSCF, also shown in Table II. The k and D^* values decreased by 56% and 45%, respectively, due to thermal ageing at 800°C for 800 hours. The decrease in k seems reasonable given the tendency of SrO to block the surface exchange process.[14] The reason for the change in D^* is not so clear, and a few possibilities are discussed here. First, it has been shown that the Sr surface segregation is accompanied by Sr depletion in the sub-surface region,[34] and this could have an impact

on bulk oxygen diffusion. Second, D^* may include a component of surface diffusion as well as bulk diffusion[28] and the former would certainly be affected by Sr surface segregation. Third, it has been shown that the processes represented by k and D^* are intimately linked, raising questions as to how readily they can be separately measured.[35,36]

Conclusions

Ageing of LSCF symmetric-electrode cells with GDC electrolytes, carried out at 800°C for 800 hours in ambient air, resulted in an increase of the electrode polarization resistance by about 120%. 3D tomographic analysis indicated no significant microstructural changes due to ageing. ICP-OES measurements of selectively dissolved surface species indicated that a Sr-rich surface phase, corresponding to 1.04 ± 0.22 atomic layers of SrO, was present, in good agreement with reports on Sr-doped perovskite-type oxide thin films. The amount of surface Sr increased by ∼3 times after the thermal ageing. Therefore, it is reasonable to conclude that Sr surface segregation, rather than microstructural changes, caused the increased LSCF polarization resistance. By applying the measured impedance response and calculated microstructural parameters to the ALS model, estimated k and D^* values were obtained. The k values was observed to decrease by ∼50% with thermal ageing, presumably explained by the increase in surface Sr. D^* was also observed to decrease by ∼50% after ageing, possibly due to Sr depletion in the sub-surface LSCF.

Acknowledgments

The authors at Northwestern University gratefully acknowledge useful conversations with Dr. Liliana V. Mogni and Dr. Zhan Gao, support by the Department of Energy (grant # DE-FG02-05ER46255), which mainly supported the ageing and electrochemical testing, and the US National Science Foundation (grant # DMR-0907639 and DMR-1506925), which mainly supported the tomography work. The work on chemical analysis is financially supported by the Austrian Science Fund (FWF) project P4509-N16 and W1243-N16. The authors also acknowledge the assistance of the Electron Probe Instrumentation Center (EPIC) at the NUANCE Center-Northwestern University, which has received support from the Soft and Hybrid Nanotechnology Experimental (SHyNE) Resource (NSF NNCI-1542205); the MRSEC program (NSF DMR-1121262) at the Materials Research Center; the International Institute for Nanotechnology (IIN); the Keck Foundation; and the State of Illinois, through the IIN. Part of the FIB-SEM was carried out at the Electron Microscopy Center for Materials Research at Argonne National Laboratory, a US Department of Energy Office of Science Laboratory operated under Contract No. DEAC02-06CH11357 by UChicago Argonne, LLC.

References

1. L. W. Tai, M. M. Nasrallah, H. U. Anderson, D. M. Sparlin, and S. R. Sehlin, *Solid State Ionics*, **76**, 259 (1995).
2. L. W. Tai, M. M. Nasrallah, H. U. Anderson, D. M. Sparlin, and S. R. Sehlin, *Solid State Ionics*, **76**, 273 (1995).
3. Y. Teraoka, H. M. Zhang, S. Furukawa, and N. Yamazoe, *Chem. Lett.*, 1743 (1985).
4. E. V. Tsipis and V. V. Kharton, *J. Solid State Electrochem.*, **12**, 1039 (2008).
5. A. Esquirol, N. P. Brandon, J. A. Kilner, and M. Mogensen, *J. Electrochem. Soc.*, **151**, A1847 (2004).
6. H. Y. Tu, M. B. Phillipps, Y. Takeda, T. Ichikawa, N. Imanishi, N. M. Sammes, and O. Yamamoto, *J. Electrochem. Soc.*, **146**, 2085 (1999).
7. Z. Pan, Q. Liu, L. Zhang, X. Zhang, and S. H. Chan, *J. Electrochem. Soc.*, **162**, F1316 (2015).
8. S. P. Jiang, S. Zhang, and Y. D. Zhen, *J. Electrochem. Soc.*, **153**, A127 (2006).
9. L. Zhao, J. Drennan, C. Kong, S. Amarasinghe, and S. P. Jiang, *J. Mater. Chem. A*, **2**, 11114 (2014).
10. Y. Liu, K. Chen, L. Zhao, B. Chi, J. Pu, and S. P. Jiang, *Int. J. Hydrogen Energy*, **39**, 15868 (2014).
11. S. P. Simner, M. D. Anderson, M. H. Engelhard, and J. W. Stevenson, *Electrochem. Solid State Lett.*, **9**, A478 (2006).
12. W. Jung and H. L. Tuller, *Energy Environ. Sci.*, **5**, 5370 (2012).
13. E. Bucher, W. Sitte, F. Klauser, and E. Bertel, *Solid State Ionics*, **208**, 43 (2012).
14. Z. Cai, M. Kubicek, J. Fleig, and B. Yildiz, *Chem. Mater.*, **24**, 1116 (2012).
15. K. Kubicek, A. Limbeck, T. Fromling, H. Hutter, and J. Fleig, *J. Electrochem. Soc.*, **158**, B727 (2011).
16. G. M. Rupp, A. Limbeck, M. Kubicek, A. Penn, M. Stöger-Pollach, G. Friedbacher, and J. Fleig, *J. Mater. Chem. A*, **2**, 7099 (2014).
17. S. B. Adler, *Chem. Rev.*, **104**, 4791 (2004).
18. X. Chen, S. Wang, Y. L. Yang, L. Smith, N. J. Wu, B. I. Kim, S. S. Perry, A. J. Jacobson, and A. Ignatiev, *Solid State Ionics*, **146**, 405 (2002).
19. L. Blum, U. Packbier, I. C. Vinke, and L. G. J. de Haart, *Fuel Cells*, **13**, 646 (2013).
20. S. B. Adler, J. A. Lane, and B. C. H. Steele, *J. Electrochem. Soc.*, **143**, 3554 (1996).
21. J. S. Cronin, K. Muangnapoh, Z. Patterson, K. J. Yakal-Kremski, V. P. Dravid, and S. A. Barnett, *J. Electrochem. Soc.*, **159**, B385 (2012).
22. J. S. Cronin, J. R. Wilson, and S. A. Barnett, *J. Power Sources*, **196**, 2640 (2011).
23. B. Münch and L. Holzer, *J. Am. Ceram. Soc.* **91**, 4059 (2008).
24. G. M. Rupp, H. Tellez, J. Druce, A. Limbeck, T. Ishihara, J. Kilner, and J. Fleig, *J. Mater. Chem. A*, **3**, 22759 (2015).
25. J. Druce, T. Ishihara, and J. Kilner, *Solid State Ionics*, **262**, 893 (2014).
26. Y. Liu, F. Wang, B. Chi, J. Pu, and S. P. Jiang, *J. Alloys and Compd.*, **578**, 37 (2013).
27. K. Yakal-Kremski, L. V. Mogni, A. Montenegro-Hernandez, A. Caneiro, and S. A. Barnett, *J. Electrochem. Soc.*, **161**, F1366 (2014).
28. Y. Lu, C. Kreller, and S. B. Adler, *J. Electrochem. Soc.*, **156**, B513 (2009).
29. J.-P. Diard, B. Le Gorrec, and C. Montella, *Handbood of Electrochemical Impedance Spectroscopy*, Bio-Logic (2012).
30. S. Havriliak and S. Negami, *Polymer*, **8**, 161 (1967).
31. Y. Fukuda, S.-i. Hashimoto, K. Sato, K. Yashiro, and J. Mizusaki, *ECS Trans.*, **25**, 2375 (2009).
32. H. J. M. Bouwmeester, M. W. Den Otter, and B. A. Boukamp, *J. Solid State Electrochem.*, **8**, 599 (2004).
33. M. H. R. Lankhorst and J. E. ten Elshof, *J. Solid State Chem.*, **130**, 302 (1997).
34. J. Druce, H. Tellez, M. Burriel, M. D. Sharp, L. J. Fawcett, S. N. Cook, D. S. McPhail, T. Ishihara, H. H. Brongersma, and J. A. Kilner, *Energy Environ. Sci.*, **7**, 3593 (2014).
35. M. A. Tamimi, A. C. Tomkiewicz, A. Huq, and S. McIntosh, *J. Mater. Chem. A.*, **2**, 18838 (2014).
36. S. McIntosh, *Faraday Discuss.*, **182**, 177 (2015).
37. B. C. H. Steele and J.-M. Bae, *Solid State Ionics*, **106** (1998).